Journal of Rare Earths 37 (2019) 1066–1071

Contents lists available at ScienceDirect

Journal of Rare Earths

journal homepage: http://www.journals.elsevier.com/journal-of-rare-earths

Magnetic properties of melt-spun ribbons $(Sm_{1-x}Zr_x)(Fe_{0.92}Ti_{0.08})_{10}$ with $ThMn_{12}$ structure and their hydrides☆

A.G. Popov [a, b], A.V. Protasov [a, b, *], V.S. Gaviko [a, b], D.A. Kolodkin [a], P.B. Terentev [a, b], E.G. Gerasimov [a, b], Tianli Zhang [c], Chengbao Jiang [c]

[a] M.N. Miheev Institute of Metal Physics of Ural Branch of Russian Academy of Sciences, Str. S. Kovalevskoy, 18 Ekaterinburg, 620990, Russia
[b] Institute of Natural Sciences and Mathematics, Ural Federal University, pr. Mira, 19 Ekaterinburg, 620002, Russia
[c] School of Materials Science and Engineering, Beihang University, Beijing 100191, China

ARTICLE INFO

Article history:
Received 20 August 2018
Received in revised form
12 April 2019
Accepted 18 April 2019
Available online 12 June 2019

Keywords:
Sm-Zr-Fe-Ti
$ThMn_{12}$
Melt-spun ribbons
Hydrogenation
Magnetic properties

ABSTRACT

The structure and magnetic hysteresis properties of the cast $Sm_{1-x}Zr_x(Fe_{0.92}Ti_{0.08})_{10}$ ($x = 0$–0.3) alloys and melt-spun ribbons prepared from them were studied. In the cast alloy with $x > 0.2$, a considerable amount of the eutectic phase is found in the SEM micrographs. Analysis of the temperature dependences of the magnetic susceptibility and XRD patterns allows amorphous state in the as-spun ribbons with $x > 0.2$ to be determined. The specific magnetization measured in a field of 17 kOe and remanence decrease with increasing annealing temperature from 800 to 900 °C and weakly depend on Zr concentration. The maximal value of coercivity $H_c = 4.7$ kOe is obtained on the ribbons with $x = 0.2$ after annealing at 850°C for 10 min. After additional hydrogenation of the ribbons, both the coercivity and remanence increase by 54% and 7%, respectively.

1. Introduction

Compounds with the stoichiometry RFe_{12} (R is a rare-earth element) and the tetragonal $ThMn_{12}$ type structure (hereafter, 1:12) attract attention as potential hard magnetic materials with low R content.[1–9] However, for the entire series of lanthanide elements, binary RFe_{12} bulk alloys with $ThMn_{12}$ type structure are impossible to synthesize. To this end, it is necessary to substitute Fe by stabilizing elements *M*. Ternary compounds $RFe_{12-x}M_x$ exist for M = Al, Si, Ti, V, Cr, Nb, Mo, and W.[1–4] Si atoms substitute for Fe atoms in the tetragonal crystal lattice of the $ThMn_{12}$ type (space group *P*4/*mmm*) structure at sites 8f (75%) and 8j[10] contrary to the other stabilizing atoms (Ti, Mo, etc.) which occupy only 8i sites[11–13] The concentration region of x in which the $RFe_{12-x}M_x$ phase is stable depends on *M*.[6] With increasing x, substitution of the stabilizing element *M* for Fe decreases the saturation magnetization $4\pi M_s$ of the $RFe_{12-x}M_x$ compounds.[14,15] However, the $ThMn_{12}$ structure remains unstable for x less than a certain critical value.[16] Nowadays, Ti is known to be the best alloying element for the stabilization of the $ThMn_{12}$ structure, since it requires the minimal content $x \approx 1$[5]. It has been announced that the anisotropy field H_a and the Curie temperature T_C of the $SmFe_{11}Ti$ compound are 198 kOe and 314 °C, respectively.[7] However, the $SmFe_{11}Ti$ compound did not receive much attention, since $4\pi M_s$ was 12.7 kG at room temperature,[7] which is significantly lower than 16 kG for $Nd_2Fe_{14}B$. Ding et al.[17] studied the hysteresis properties of the $SmFe_{11.75}Ti_{1.04}$ ribbons prepared by spinning. After annealing at 800 °C, the values of coercivity H_c and specific remanence σ_r were 5.8 kOe and 56.2 emu/g, respectively. With increasing annealing temperature up to 900°C, a decrease of H_c and an increase of σ_r were observed. Authors explained such behavior of the magnetic characteristics by the occurrence of an additional α-Fe phase.

Du et al. studied the effect of substitution of Zr for Mo on the structure and magnetic properties of a series of $NdFe_{10.5}Mo_{1.5-x}Zr_x$ compounds.[18] As a result, it has been found that Zr atoms substitute Nd atoms at 2*a* sites rather than Mo atoms at 8*i* sites. Recently, Suzuki et al.,[19] Kunoet al.[20] and Tozman et al.[21] have shown that the tetragonal structure of the $ThMn_{12}$ type can develop in the $Sm(Fe,Co,Ti)_{12}$ alloys at the low content of titanium ($x = 0.5$), if to

☆ **Foundation item:** Project supported by BRICS STI Framework Program for Basic Research (RFFI-BRICS) (17-52-80072), NSFC-BRICS (51761145026) and the State Assignment of Ministry of Education and Science of the Russian Federation (topic "Magnet") (AAAA-A18-118020290129-5).

* Corresponding author. M.N. Miheev Institute of Metal Physics of Ural Branch of Russian Academy of Sciences, Str. S. Kovalevskoy, 18 Ekaterinburg, 620990, Russia.
E-mail address: protasov@imp.uran.ru (A.V. Protasov).

https://doi.org/10.1016/j.jre.2019.04.007
1002-0721/

partially substitute Zr for Sm. The hard-magnetic characteristics of such alloys are found to be highly attractive ($4\pi M_s$ = 15.3 kG, H_a = 84 kOe, and T_C = 557 °C). The magnets made from these alloys would show high thermal stability of hysteresis properties compared with Nd-Fe-B based magnets.

It is known that after hydrogenation of $RFe_{11}Ti$ alloys, the $ThMn_{12}$ crystal lattice is retained and the unit-cell volume increases by about 1%.[22,23] From the analysis of neutron diffraction data,[24,25] it has been derived that the H atoms partially fill up the interstitial 2*b* sites. The 2*b* sites are formed by two rare earth atoms and four iron atoms at site 8*j*. The increase of interatomic spacings of Fe–Fe results in enhanced exchange interactions between iron atoms and growth of the Curie temperature T_c and magnetic moment at Fe atom.[23] Bringing H atoms into close contact with the rare-earth atoms in $SmTiFe_{11}H_x$ leads to drastic changes in the rare-earth sublattice anisotropy. According to literature,[22,23,26] the anisotropy field after hydrogenation can be increased by 20%.

The formation of the nanocrystalline $ThMn_{12}$ structure can enhance magnetic hysteresis properties of the alloys. Therefore, in this work, we studied magnetic and crystallographic properties of the (SmZr)-Fe-Ti alloys, melt-spun ribbons and their hydrides.

2. Experimental

The $Sm_{1-x}Zr_x(Fe_{0.92}Ti_{0.08})_{10}$ alloys with x = 0–0.3 were prepared by induction melting of pure metals (no less than 99.9% in purity) in alumina crucibles in the argon atmosphere. In order to compensate for material interaction with the crucible in the course of melting, 5 wt% of excessive Sm was added. The ribbons were prepared by melt spinning on the copper wheel rotating at the velocity V_s = 30 m/s. The ribbons were annealed at the temperatures of 750–900 °C in the argon atmosphere. In order to enhance coercivity H_c, some annealed ribbons were subjected to hydrogenation at 200°C for 5 h. XRD investigations were performed using a multifunctional Empyrean (PANanalytical) diffractometer with monochromated Cu Kα radiation. Diffraction patterns were analyzed with the software "Powder cell" and "HighScore Plus". The average grain size of the nanocrystalline phase was determined according to the broadening of their diffraction peaks, employing the Williamson-Hall method.[27] Temperature dependences of the magnetic susceptibility $\chi(T)$ were measured in ac magnetic field with an amplitude of 4 Oe and frequency of 800 Hz in the temperature range of 18–880°C. The magnetic properties of the samples were investigated using a vibrating sample magnetometer (VSM, Lake Shore 7407) with the maximum field of 17 kOe, as well as in high pulsed magnetic fields with the strength of up to 210 kOe. The scanning-electron microscopy and EDS were performed by using a microscope Quanta 200.

3. Results and discussion

Fig. 1(a–d) demonstrate the microstructure of the cast $(Sm_{1-x}Zr_x)(Fe_{0.92}Ti_{0.08})_{10}$ alloys. Chemical compositions of the phases determined by SEM/EDX method are listed in Table 1. The composition of the main phase (A) in all alloys is close to the stoichiometry of 1:12. The temperature dependences of the magnetic susceptibility $\chi(T)$ (Fig. 2(a, b)) have a peak in the vicinity of the Curie temperature of 316 °C.

With increasing x, the Zr content in the 1:12 phase increases, whereas the T_C values decrease. However, Zr introduced into the alloy is localized not only in the 1:12 phase but partially in additional phases. The alloys with x = 0 and 0.1 contain, along with the main 1:12 phase, a small amount of dark inclusions (B) of the $Fe_{2+\delta}Ti/Fe_{2+\delta}(Ti,Zr)$ phase which has a wide homogeneity region. The size of these inclusions is about 10 μm. Refractory inclusions of $Fe_{2+\delta}Ti/Fe_{2+\delta}(Ti,Zr)$ solidify at a temperature above 1400°C. After the subsequent cooling, the liquid enriched in samarium, in which the inclusions are immersed, solidifies with the formation of regions (C) composed of the $Sm(Fe,Ti)_z/(Sm,Zr)(Fe,Ti)_z$ phases of the alternating composition with $3 < z < 8$.

The microstructure of the alloys with $x \geq 0.2$ is shown in Fig. 1(c and d); it contains the eutectic phase (D), the volume fraction of which can be up to 40%. In the ternary Sm-Fe-Ti alloys, the eutectic can form as a result of the complex transition L → α-Fe + $Sm(Fe,Ti)_{12}$+Fe_2Ti[28] at the Sm content less than that of our alloys (x = 0 and 0.1). The decrease in the Sm content due to an increase in the Zr content causes the formation of the eutectic. The alloy with x = 0.3 contains additional amount of the primary crystals of α-Fe (E), which can be judged by an increase of its contribution into $\chi(T)$ ($T_C \approx$ 770°C, Fig. 2(d)).

After homogenizing annealing at 1050°C for 15 h, the alloys become virtually single-phase. Fig. 3 presents the results of measurements of the specific magnetization for the magnetically aligned powders with x = 0 and 0.3 and their hydrides, the size of particles being less than 40 μm. The measurements were carried out along $\sigma_{||}$ and perpendicular $\sigma_{\perp}$ the axis of alignment. The coercivity of the powders oriented along the texture axis does not exceed 0.25 kOe. The saturation magnetization σ_s has been obtained by extrapolation of $\sigma_{||}$ vs $1/H^2$. The anisotropy field H_a have been derived as described elsewhere.[29] The data on the σ_s and H_a

Table 1
Chemical composition of the cast $(Sm_{1-x}Zr_x)(Fe_{0.92}Ti_{0.08})_{10}$ alloys according to SEM/EDX.

x (Zr)	Phase	Label in Fig. 1	Chemical composition fromEDX
0	1:12	A	$Sm(Fe_{0.92}Ti_{0.08})_{11.2}$
	$Fe_{2+\delta}Ti$	B	$Fe_{2.6}Ti$
	$Sm(Fe,Ti)_z$	C	$Sm(Fe_{0.93}Ti_{0.07})_{7.6}$
0.1	1:12	A	$(Sm_{0.91}Zr_{0.09})(Fe_{0.92}Ti_{0.08})_{10.7}$
	$Fe_{2+\delta}(Ti,Zr)$	B	$Fe_{2.9}(Ti_{0.75}Zr_{0.25})$
	$(Sm,Zr)(Fe,Ti)_z$	C	$(Sm_{0.79}Zr_{0.21})(Fe_{0.88}Ti_{0.12})_{4.6}$
0.2	1:12	A	$(Sm_{0.84}Zr_{0.16})(Fe_{0.93}Ti_{0.07})_{9.9}$
	eutectic	D	$(Sm_{0.63}Zr_{0.37})(Fe_{0.90}Ti_{0.10})_{12.6}$
0.3	1:12	A	$(Sm_{0.77}Zr_{0.23})(Fe_{0.93}Ti_{0.07})_{9.7}$
	eutectic	D	$(Sm_{0.63}Zr_{0.37})(Fe_{0.90}Ti_{0.10})_{13.0}$
	α-Fe	E	–

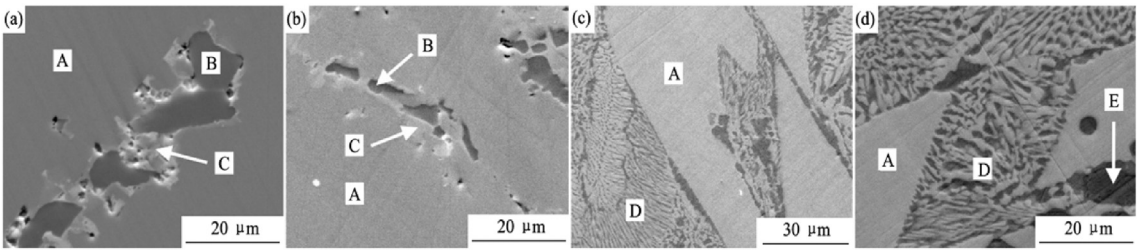

Fig. 1. SEM microstructures of the cast $(Sm_{1-x}Zr_x)(Fe_{0.92}Ti_{0.08})_{10}$ alloys: (a) x = 0; (b) x = 0.1; (c) x = 0.2; (d) x = 0.3.

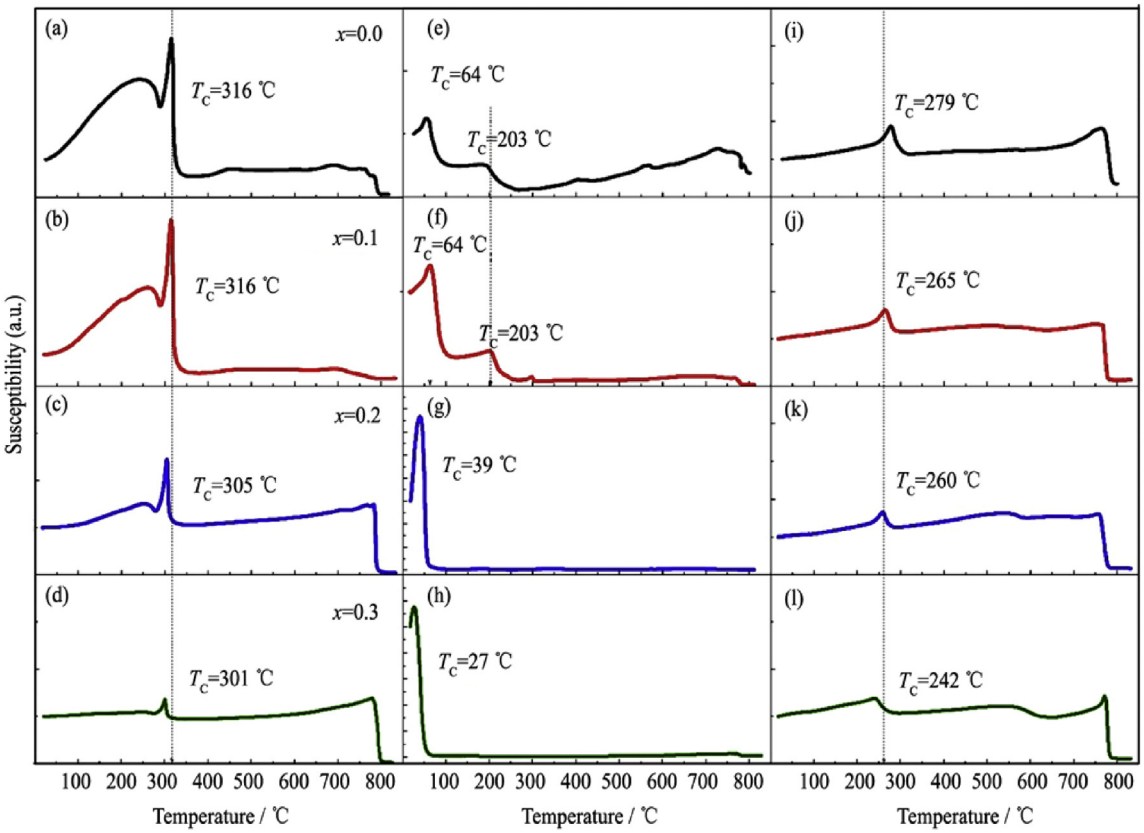

Fig. 2. Temperature dependences of magnetic susceptibility $\chi(T)$ of cast alloys (a–d), as-spun ribbons (e–h), and ribbons annealed at 800 °C, 10 min (i–l).

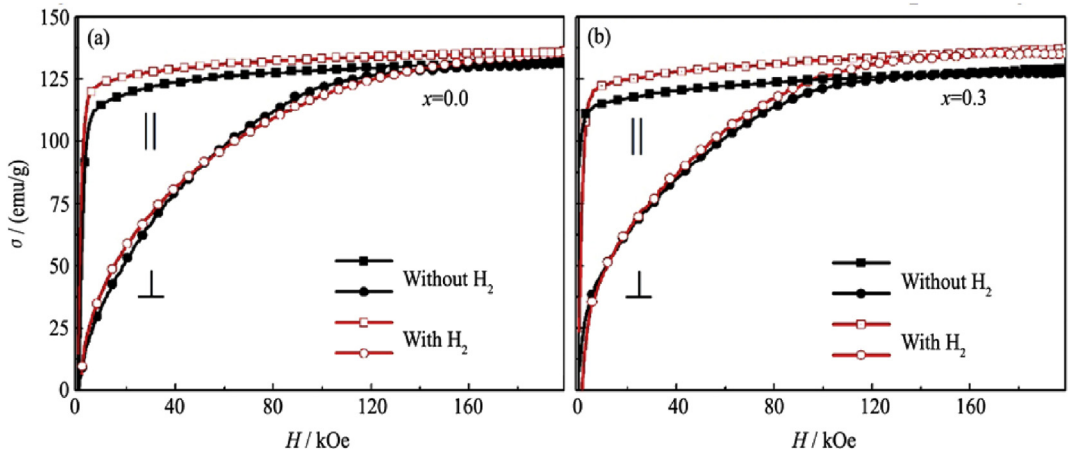

Fig. 3. Magnetization curves of aligned powders of $Sm_{1-x}Zr_x(Fe_{0.92}Ti_{0.08})_{10}$ alloys and their hydrides at room temperature.

Table 2
Data on the specific magnetization and anisotropy field for the $Sm_{1-x}Zr_x(Fe_{0.92}Ti_{0.08})_{10}$ powders prior to and after hydrogenation.

Powder	$x = 0.0$		$x = 0.1$		$x = 0.2$		$x = 0.3$	
	σ_s (emu/g)	H_a (kOe)	σ_s (emu/g)	H_a (kOe)	σ_s (emu/g)	H_a (kOe)	σ_s (emu/g)	H_a (kOe)
Without H_2	122	140	121	136	117	129	116	125
With H_2	127	170	125	162	124	145	123	136

are given in Table 2. The value of H_a for $x = 0$ agrees well with the earlier published data[22,23,26] and insignificantly decreases with increasing concentration of Zr, according to the data of Ref. 21. After hydrogenation, the values of σ_s of powders grow by 5%, on average, whereas increment of H_a gradually decreases from 30 to 11 kOe as x increases from 0 to 0.3, respectively.

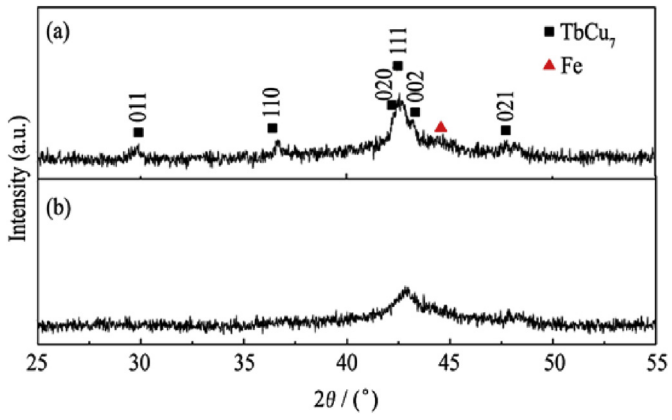

Fig. 4. XRD patterns of as-spun ribbons $Sm_{0.9}Zr_{0.1}(Fe_{0.92}Ti_{0.08})_{10}$ (a) and $Sm_{0.7}Zr_{0.3}(Fe_{0.92}Ti_{0.08})_{10}$ (b).

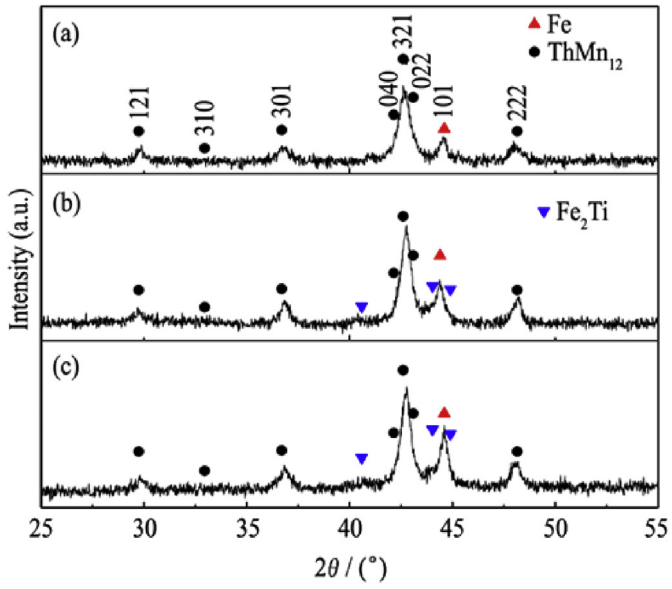

Fig. 5. XRD patterns of the $Sm(Fe_{0.92}Ti_{0.08})_{10}$ (a) and $Sm_{0.7}Zr_{0.3}(Fe_{0.92}Ti_{0.08})_{10}$ (b) ribbons annealed at 800 °C 10 min, and $Sm_{0.7}Zr_{0.3}(Fe_{0.92}Ti_{0.08})_{10}$ after additional hydrogenation (c).

According to the magnetic susceptibility measurements shown in Fig. 2(e, f), the as-spun ribbons with $x = 0$ and 0.1 contain several phases: amorphous phase with the $T_C = 64$ °C, disordered phase with the $TbCu_7$-type structures with $T_C = 203$ °C,[30] and α-Fe with $T_C \approx 770$ °C. Fig. 4(a) shows the X-ray diffraction pattern measured on a ribbon with $x = 0.1$ at room temperature where amorphous halo and broadening of the reflections of the $TbCu_7$-type structure[31] and α-Fe are also observed. The melt-spinning at the speed $V_s = 30$ m/s suppresses the ordering of the Fe(Ti) atomic pairs, which results in the formation of the disordered $TbCu_7$-type structures instead of the $ThMn_{12}$ one. The volume fraction of the disordered phase in these ribbons reaches 20%. The XRD measurements allowed us to conclude that the as-spun ribbons with $x \geq 0.2$ are fully amorphous. This is evidenced by only one maximum in the $\chi(T)$ dependences of the alloys with $x = 0.2$ and 0.3 in Fig. 2(h, g), respectively, and the existence of a broad halo in the diffraction pattern of the ribbons with $x = 0.3$ (Fig. 4(b)). The formation of the eutectic in the as-cast alloys favors the formation of amorphous state in the melt-spun ribbons with $x \geq 0.2$.

All of the $\chi(T)$ curves of the melt-spun ribbons annealed at 800 °C for 10 min (Fig. 2(i – l)) show two distinct magnetic transitions at the points T_C of the 1:12 and α-Fe phases. The T_C values of the 1:12 phase of the annealed ribbons are by 40–50 °C lower than that of the same phase in the initial cast alloys. Besides, with increasing x, T_C of the 1:12 phase in the melt-spun ribbons decreases faster than in the cast alloys. It can be caused by an insufficient order of the dumbbell pairs of Fe–Fe(Ti) in the 1:12 structure and an increase in the Zr solubility in the 1:12 phase of the annealed ribbons.

The X-ray patterns of the annealed ribbons with $x = 0$ and 0.3, which are demonstrated in Fig. 5(a, b), also prove the existence of the tetragonal 1:12 phase and α-Fe. Approximately 1% of the Fe_2Ti phase was found in the annealed ribbons with $x = 0.3$ (Fig. 5(b)). After the annealing and additional hydrogenation, the melt-spun ribbons with $x = 0.3$ have the same phase composition (Fig. 5(c)). The volume fraction and lattice parameters of the phases of $Sm_{1-x}Zr_x(Fe_{0.92}Ti_{0.08})_{10}$ samples are listed in Table 3. The average grain size measured from XDA decreased from 84 ± 5 to 68 ± 5 nm with increasing x from 0 to 0.3, respectively.

An increase in the Zr content gives rise to the volume fraction of the α-Fe. The substitution of a Sm atom with a radius of 0.1822 nm by a Zr atom with a radius of 0.1602 nm results in the decrease of the lattice parameters a and c of the 1:12 phase. The hydrogenation of the annealed ribbons leads to the opposite result. Interstitial hydrogen atoms at sites 2b of the 1:12-phase crystal lattice of the ribbons with $x = 0.3$ enlarge the unit cell in volume by 1.7%.

In Fig. 6, the microstructure of fractures of the ribbons with $x = 0.2$, both as-spun and annealed at 850 °C 10 min, are shown. The fracture of the amorphous ribbon shown in Fig. 6(a) is likely to occur at colonies of the dendrites. Fig. 6(b) shows the granular structure of the annealed ribbons with the average grain size of about 1 μm.

Fig. 7 demonstrates the demagnetization curves of the $Sm_{1-x}Zr_x(Fe_{0.92}Ti_{0.08})_{10}$ ribbons, both as-spun and annealed at 800°C for 10 min. Immediately after the melt spinning, the coercivity of the ribbons is low. The value of maximal specific magnetization measured in the field of 17 kOe (σ_{17}) decreases win increasing x. The quasi-crystalline as-spun ribbons with $x < 0.2$ obviously fail to reach saturation at 17 kOe. The amorphous ribbons with $x \geq 0.2$ tend to become magnetized easier. Increasing the annealing temperature up to 700°C results in the structural transitions from the disordered $TbCu_7$-type phase and from the amorphous phase into the hard magnetic 1:12 phase. As is shown in

Table 3
Phase composition and lattice parameters of particular melt-spun ribbons.

x (Zr)	Heat treatment	Phase composition	Phase-volume fraction	Lattice parameters		
				a (nm)	c (nm)	c/a
0	800 °C, 10 min	1:12	88.0	0.8496(2)	0.4863(2)	0.572
		α-Fe	12.0	0.2874(1)	–	–
0.3	800 °C, 10 min	1:12	79.7	0.8440(2)	0.4850(2)	0.575
		α-Fe	20.3	0.2874(1)	–	–
0.3	800 °C, 10 min + 200 °C, 5 h in H_2	1:12	80.3	0.8474(2)	0.4872(2)	0.575
		α-Fe	19.7	0.2874(1)	–	–

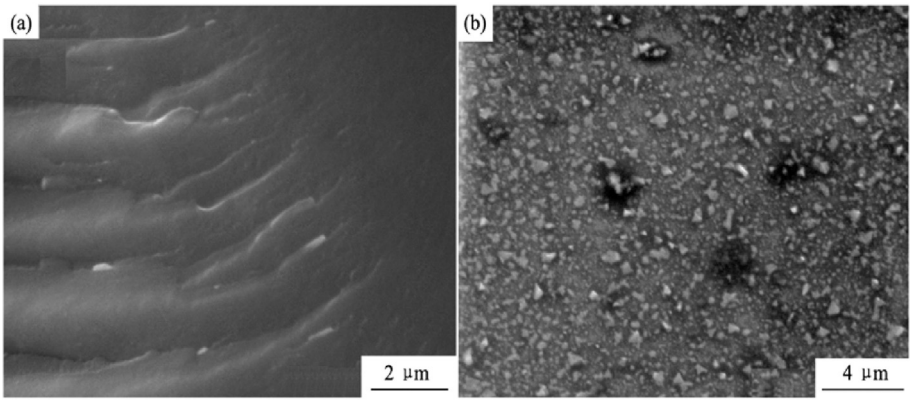

Fig. 6. SEM micrographs of fractured surface of as-spun (a) and annealed at 850 °C, 10 min (b) $Sm_{0.8}Zr_{0.2}(Fe_{0.92}Ti_{0.08})_{10}$ ribbons.

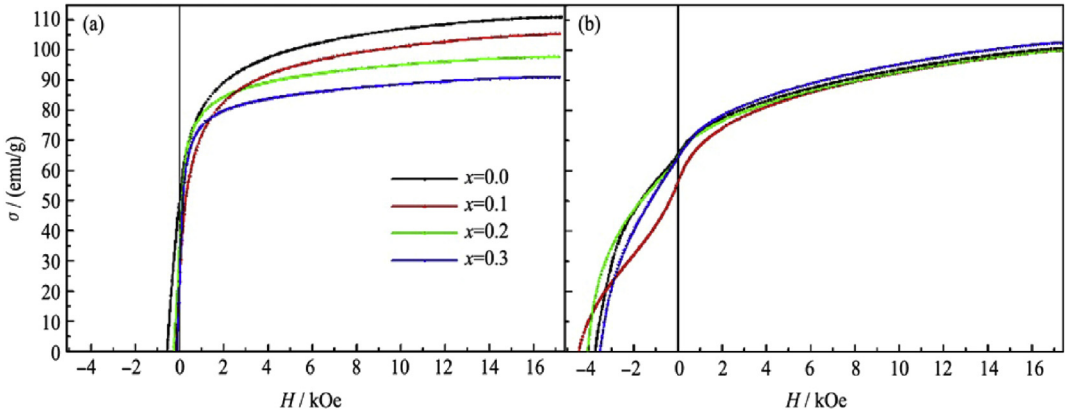

Fig. 7. Demagnetization curves of the as-spun (a) and annealed at 800 °C, 10 min (b) $Sm_{1-x}Zr_x(Fe_{0.92}Ti_{0.08})_{10}$ ribbons.

Fig. 6(b), the average grain size of the 1:12 phase is no more than 100 nm. The coercivity starts drastically increasing. In Fig. 7(b), the demagnetization curves of the ribbons annealed at 800°C for 10 min are shown. The values of σ_{17} fall in the range from 100 to 103 emu/g. In comparison to the as-spun ribbons, these values are decreased for the ribbons with $x < 0.2$ and increased for ribbons with $x \geq 0.2$. This is likely to be ascribed to the above-described structural transitions from the disordered $TbCu_7$-type phase and from the amorphous phase into the hard magnetic 1:12 phase. Since the easy-magnetization axes of the nanocrystalline grains of the high-anisotropy 1:12 phase are randomly oriented, the magnetic saturation cannot be reached in the field of 17 kOe. The ratio of the residual specific magnetization to the saturation magnetization, σ_r/σ_s, for the samples with $x = 0.1$–0.3 makes up 0.55, which indicates that in these nanocrystalline ribbons, the remanence is enhanced due to the intergrain exchange coupling. The coercivity of the ribbons annealed at 800 °C increases up to about 4 kOe.

Fig. 8 shows the dependences of the parameters of the demagnetization curves on the Zr content and annealing temperature. The maximal specific magnetization measured in a field 17 kOe (σ_{17}), and remanence σ_r weakly depend on the Zr concentration and gradually decrease with increasing annealing temperature from 800 to 900 °C. The maximal value of $H_c = 4.7$ kOe was found for the ribbons with $x = 0.2$ annealed at 850 °C within 10 min. The appearance of a maximum in the dependence $H_c(x)$ is traceable to the presence of two factors that affect oppositely on increasing Zr concentration. They are the decrease in the grain size, which increases the coercivity, and the decrease in the anisotropy field, which results in its lowering.

It was established that the values of σ_s and H_a of the textured powders $Sm_{1-x}Zr_x(Fe_{0.92}Ti_{0.08})_{10}$ increased after hydrogenation. In view of this fact, in order to enhance H_c, the ribbons annealed at

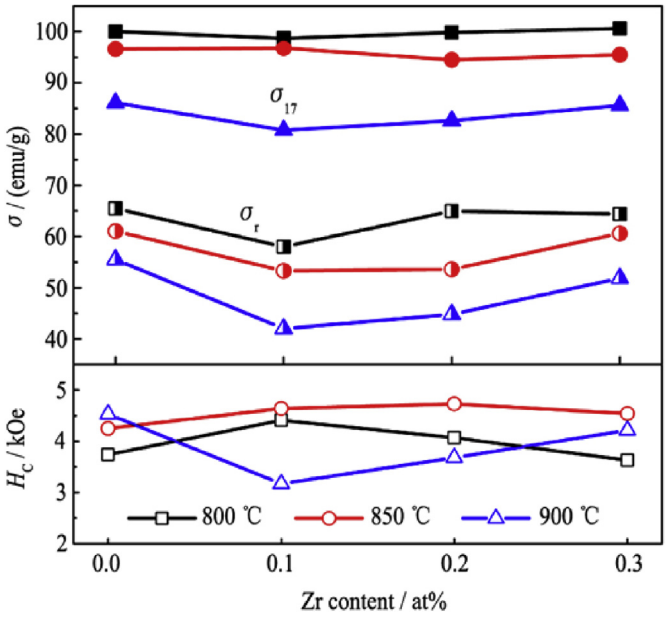

Fig. 8. Concentration dependences of specific magnetization measured in a field of 17 kOe σ_{17}, remanence σ_r and coercivity of the $Sm_{1-x}Zr_x(Fe_{0.92}Ti_{0.08})_{10}$ ribbons annealed at 800, 850 and 900 °C for 10 min.

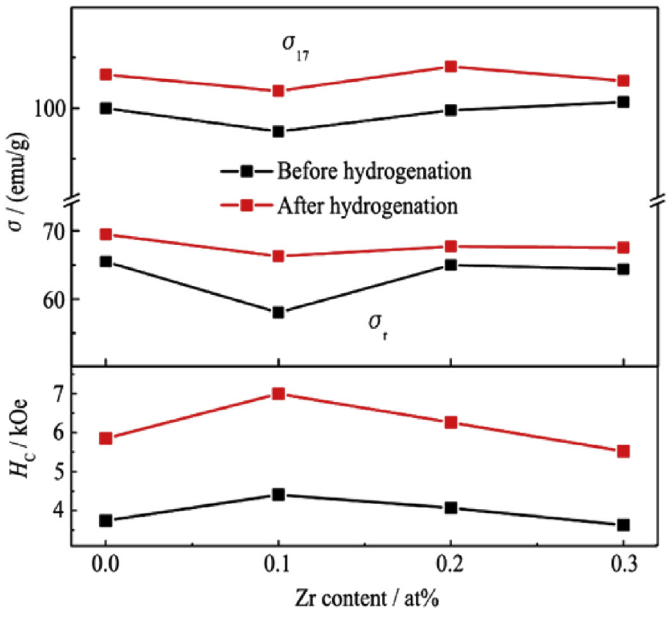

Fig. 9. Comparison of dependences of specific magnetization σ_{17}, remanence σ_r and coercivity of $Sm_{1-x}Zr_x(Fe_{0.92}Ti_{0.08})_{10}$ ribbons annealed at 800 °C on Zr content before and after hydrogenation.

800 °C for 10 min were subjected to hydrogenation at 200°C for 5 h. Fig. 9 demonstrates that after hydrogenation the magnetic-hysteresis properties enhance for the entire range of Zr concentrations. For instance, at $x = 0.2$, the values of σ_{17}, σ_r and H_c increase on the average by 4%, 7% and 54%, respectively. If the properties of this nanocrystalline rare-earth-lean alloy could be reproduced in a three-dimensional bulk magnet, the latter would exhibit a remanence B_r of 6.2 kG and a maximum energy product $(BH)_{max}$ of 6.1 MGOe. Unfortunately, the absence of texture in these alloys does not allow an increase in the magnetic hysteresis properties to be gained.

4. Conclusions

The cast $(Sm_{1-x}Zr_x)(Fe_{0.92}Ti_{0.08})_{10}$ alloys contain the main $ThMn_{12}$-type phase, Fe_2Ti, and $(Sm,Zr)_2(Fe,Ti)_{17}$ inclusions. With increasing x up to 0.2, a eutectic structure was observed in the micrographs. At $x < 0.2$, the as-spun $(Sm_{1-x}Zr_x)(Fe_{0.92}Ti_{0.08})_{10}$ ribbons consist of a mixture of amorphous, disordered $TbCu_7$-type and α-Fe phases. The amorphous phase was detected only in the ribbons with $x \geq 0.2$. After the annealing, all ribbons contain the tetragonal $ThMn_{12}$ phase and α-Fe. The specific saturation magnetization σ_s and anisotropy field H_a of the magnetically aligned $(Sm_{1-x}Zr_x)(Fe_{0.92}Ti_{0.08})_{10}$ powders insignificantly decrease with increasing concentration of Zr. After hydrogenation, the values of σ_s and H_a of the powders grow up. The values of σ_s increase by 5%, on average, whereas increment of H_a, gradually decreases from 30 to 11 kOe as x increases from 0 to 0.3, respectively. The specific magnetization measured in a field of 17 kOe σ_{17} and remanence σ_r of the annealed ribbons weakly depend on the Zr concentration and gradually decrease with increasing annealing temperature from 800 to 900 °C. The maximal value of coercivity $H_c = 4.7$ kOe is found in the spun ribbons with $x = 0.2$ after the annealing at 850 °C. After hydrogenation the coercivity of all annealed ribbons is increased by 40%–60%.

Acknowledgments

The X-ray diffraction investigation and the magnetic measurements have been performed in the Center of Collaborative Access of IMP UB RAS.

References

1. Felner I, Nowik I, Seh M. Ferrimagnetism and hyperfine interactions in RFe_5Al_7 (R = rare earth). *J Magn Magn Mater*. 1983;38(2):172.
2. Ohashi K, Yokoyama T, Osugi R, Tawara Y. The magnetic and structural properties of R-Ti-Fe ternary compounds. *IEEE Trans Magn*. 1987;23(5):3101.
3. De Mooij DB, Buschow KHJ. Some novel ternary $ThMn_{12}$-type compounds. *J Less Common Met*. 1988;136(2):207.
4. Fuquan B, Wang JL, Tegus O, Dagula W, Tang N, Yang FM, et al. Phase formation and magnetic properties of $YFe_{12-x}Nb_x$ (x=0.70–0.90) compounds. *J Magn Magn Mater*. 2005;290–291:1192.
5. Verhoef R, de Boer FR, Zhang ZD, Buschow KHJ. Moment reduction in $RFe_{12-x}T_x$ compounds (R=Gd, Y and T=Ti, Cr, V, Mo, W). *J Magn Magn Mater*. 1988;75(3):319.
6. Coehoorn R. Electronic structure and magnetism of transition-metal-stabilized $YFe_{12-x}M_x$ intermetallic compounds. *Phys Rev B*. 1990;41(17):11790.
7. Kim HT, Kim YB, Kim CS, Jin H. Magnetocrystalline anisotropy of $(Sm_{0.5}RE_{0.5})Fe_{11}Ti$ compounds (RE = Ce, Pr, Nd, Sm, Gd and Tb). *J Magn Magn Mater*. 1996;152(3):387.
8. Zhao L, Yang H, Yu L, Cui YM, Zhao XP, Zou B, et al. Structure and magnetic properties of nanocrystalline $CoLa_{0.08}Fe_{1.92}O_4$ ferrite. *J Magn Magn Mater*. 2006;301(2):445.
9. Yang J, Yang Y. *Magnetic properties and interstitial atom effects in the R(Fe,M)$_{12}$ compounds. Handbook of advanced magnetic materials*. Boston, MA: Springer US; 2006:1414.
10. Sun GA, Chen B, Du HL, Fan ZJ, Gao T, Qi XH. Electronic structure and magnetism of $R(Fe,Si)_{12}$ (R = Y, Nd). *Sci China, Ser A G*. 2006;49(2):195.
11. Ohashi K, Tawara Y, Osugi R, Sakurai J, Komura Y. Identification of the intermetallic compound consisting of Sm, Ti, Fe. *J Less Common Met*. 1988;139(2):L1.
12. Buschow KHJ. Structure and properties of some novel ternary Fe-rich rare-earth intermetallics (invited). *J Appl Phys*. 1988;63(8):3130.
13. Psycharis V, Christides C. Frank–Kasper polyhedra, disclination nets and basic magnetism in $Nd_3(Fe,Ti)_{29}$ and $Nd_3(Fe,Ti)_{29}N_x$ intermetallics. *J Phys Condens Matter*. 2003;15(46):7953.
14. Miyake T, Terakura K, Harashima Y, Kino H, Ishibashi S. First-principles study of magnetocrystalline anisotropy and magnetization in $NdFe_{12}$, $NdFe_{11}Ti$, and $NdFe_{11}TiN$. *J Phys Soc Japan*. 2014;83(4), 043702.
15. Harashima Y, Terakura K, Kino H, Ishibashi S, Miyake T. First-principles study on stability and magnetism of $NdFe_{11}M$ and $NdFe_{11}MN$ for M = Ti, V, Cr, Mn, Fe, Co, Ni, Cu, Zn. *J Appl Phys*. 2016;120(20):203904.
16. Jin ZQ, Sun XK, Liu W, Zhao XG, Xiao QF, Sui YC, et al. Dependence of magnetic properties on microstructure in mechanically alloyed Nd-Fe-Ti-N. *J Magn Magn Mater*. 1997;169(1–2):135.
17. Ding J, Rosenberg M. Magnetic properties of melt spun and crystallized $SmFe_{11.75}Ti_{1.04}$. *J Magn Magn Mater*. 1989;80(1):105.
18. Du H, Han J, Zhang W, Wang CS, Wang WC, Liu SQ, et al. Determination of the zirconium site in zirconium-substituted $Nd(Fe,Mo,Zr)_{12}$ compounds. *J Magn Magn Mater*. 2004;283(2–3):316.
19. Suzuki S, Kuno T, Urushibata K, Kobayashi K, Sakuma N, Washio K, et al. A new magnet material with $ThMn_{12}$ structure: $(Nd_{1-x}Zr_x)(Fe_{1-y}Co_y)_{11+z}Ti_{1-z}N_\alpha$ (α =0.6–1.3). *J Magn Magn Mater*. 2016;401:259.
20. Kuno T, Suzuki S, Urushibata K, Kobayashi K, Sakuma N, Yano M, et al. $(Sm,Zr)(Fe,Co)_{11.0\text{-}11.5}Ti_{1.0\text{-}0.5}$ compounds as new permanent magnet materials. *AIP Adv*. 2016;6(2):0.
21. Tozman P, Sepehri-Amin H, Takahashi YK, Hirosawa S, Hono K. Intrinsic magnetic properties of $Sm(Fe_{1-x}Co_x)_{11}Ti$ and Zr-substituted $Sm_{1-y}Zr_y(Fe_{0.8}Co_{0.2})_{11.5}Ti_{0.5}$ compounds with $ThMn_{12}$ structure toward the development of permanent magnets. *Acta Mater*. 2018;153:354.
22. Nikitin SA, Tereshina IS, Verbetsky VN, Salamova AA. Transformations of magnetic phase diagram as a result of insertion of hydrogen and nitrogen atoms in the crystalline lattice of R_2Fe_{17} compounds. *J Alloys Compd*. 2002;336(1–2):36.
23. Zhang LY, Wallace WE. Structural and magnetic properties of $RTiFe_{11}$ and their hydrides (R = Y, Sm). *J Less Common Met*. 1989;149:371.
24. Isnard O, Miraglia S, Guillot M, Fruchart D. Hydrogen effects on the magnetic properties of $RFe_{11}Ti$ compounds. *J Alloys Compd*. 1998;275–277:637.
25. Mao WH, Yang JB, Cui B, Cheng BP, Yang YC, Du HL, et al. A study on the effect of hydrogen in the compounds with $ThMn_{12}$-type structure. *J Phys Condens Matter*. 1998;10(12):2611.
26. Isnard O, Guillot M, Miraglia S, Fruchart D. High field magnetization measurements of $SmFe_{11}Ti$ and $SmFe_{11}TiH_{1-\delta}$. *J Appl Phys*. 1996;79(8):5542.
27. Williamson G, Hall W. X-ray line broadening from filed aluminium and wolfram. *Acta Metall*. 1953;1(1):22.
28. Raghavan V. Fe-Sm-Ti (Iron-Samarium-Titanium). *J Phase Equilibria*. 2000;21(5):464.
29. Durst K-D, Kronmüller H. Determination of intrinsic magnetic material parameters of $Nd_2Fe_{14}B$ from magnetic measurements of sintered $Nd_{15}Fe_{77}B_8$ magnets. *J Magn Magn Mater*. 1986;59(1–2):86.
30. Yan WI, Quan NT, Luo Y, Yu DB, Wang ZL, Wu GY, et al. Structure and hard magnetic properties of $TbCu_7$-type $SmFe_{8.95-x}Ga_{0.26}Nb_x$ nitrides. *J Rare Earths*. 2018;36(2):165.
31. Wu GY, Li HW, Yu DB, Li KS, Yan WL, Yuan C, et al. Effect of niobium substitution on microstructures and thermal stability of $TbCu_7$-type Sm–Fe–N magnets. *J Rare Earths*. 2018;36(3):281.